PCI-24781 Induces Caspase and Reactive Oxygen Species–Dependent Apoptosis Through NF-κB Mechanisms and Is Synergistic with Bortezomib in Lymphoma Cells

Savita Bhalla,[1] Sriram Balasubramanian,[2] Kevin David,[1] Mint Sirisawad,[2] Joseph Buggy,[2] Lauren Mauro,[1] Sheila Prachand,[1] Richard Miller,[2] Leo I. Gordon,[1] and Andrew M. Evens[1]

Abstract

Purpose: We investigated the cytotoxicity and mechanisms of cell death of the broad-spectrum histone deacetylase (HDAC) inhibitor PCI-24781, alone and combined with bortezomib in Hodgkin lymphoma and non-Hodgkin lymphoma cell lines and primary lymphoproliferative (CLL/SLL) cells.

Experimental Design: Apoptosis, mitochondrial membrane potential, cell cycle analysis, and reactive oxygen species (ROS) were measured by flow cytometry, whereas caspase activation was determined by Western blot. Nuclear factor κB (NF-κB)-related mRNAs were quantified by reverse transcription-PCR, NF-κB–related proteins by Western blotting, and NF-κB DNA-binding activity by electromobility shift assay. Finally, gene expression profiling was analyzed.

Results: PCI-24781 induced concentration-dependent apoptosis that was associated with prominent G_0/G_1 arrest, decreased S-phase, increased p21 protein, and increased ROS in Hodgkin lymphoma and non-Hodgkin lymphoma cell lines. Dose-dependent apoptosis with PCI-24781 was also seen among primary CLL/SLL cells. PCI-24781–induced apoptosis was shown to be ROS- and caspase-dependent. Combined PCI-24781/bortezomib treatment resulted in strong synergistic apoptosis in all non-Hodgkin lymphoma lines (combination indices, 0.19-0.6) and was additive in Hodgkin lymphoma and primary CLL/SLL cells. Further, PCI-24781/bortezomib resulted in increased caspase cleavage, mitochondrial depolarization, and histone acetylation compared with either agent alone. Gene expression profiling showed that PCI-24781 alone significantly down-regulated several antioxidant genes, proteasome components, and NF-κB pathway genes, effects that were enhanced further with bortezomib. Reverse transcription-PCR confirmed down-regulation of NF-κB1 (p105), c-Myc, and IκB-kinase subunits, where NF-κB DNA binding activity was decreased.

Conclusion: We show that PCI-24781 results in increased ROS and NF-κB inhibition, leading to caspase-dependent apoptosis. We also show that bortezomib is synergistic with PCI-24781. This combination or PCI-24781 alone has potential therapeutic value in lymphoma.

Lymphoid malignancies are caused in part by genetic and epigenetic deregulation of tumor suppressor genes (1). The process of histone deacetylation is a well-characterized epigenetic modification (2, 3). Histone deacetylases (HDAC) and histone acetylases are enzymes that have been shown to be aberrantly expressed or regulated in malignant tissues, resulting in the inhibition of certain tumor suppressor genes, thereby allowing expression of the malignant phenotype. By inhibiting deacetylation of histones and allowing acetyl groups to remain on histones, HDAC inhibitors promote an open chromatin structure that allows gene transcription in relevant tumor suppressor genes that may favor tumor cell apoptosis.

The biological effects of HDAC inhibitors include reversion of the transformed phenotype, inhibition of proliferation, cell cycle arrest, induction of differentiation, and apoptosis in tumor cell lines (4–6). They have also been shown to generate reactive oxygen species (ROS) in solid tumor and leukemia cells (5, 7–9), which may contribute to the mechanism. The broad-spectrum HDAC inhibitor PCI-24781 (Pharmacyclics, Inc.) is a phenyl hydroxamic acid-based, orally bioavailable compound currently in clinical trials for the treatment of neoplastic diseases (10, 11). It has activity in solid tumors, including colorectal

Authors' Affiliations: [1]Division of Hematology/Oncology, Northwestern University Feinberg School of Medicine and the Robert H. Lurie Comprehensive Cancer Center, Chicago, Illinois and [2]Pharmacyclics Inc. Sunnyvale, California

Received 9/12/08; revised 1/12/09; accepted 1/15/09; published OnlineFirst 5/5/09.

Grant support: National Cancer Institute, K23 CA109613-A1 (A.M. Evens).
The costs of publication of this article were defrayed in part by the payment of page charges. This article must therefore be hereby marked *advertisement* in accordance with 18 U.S.C. Section 1734 solely to indicate this fact.

Note: Supplementary data for this article are available at Clinical Cancer Research Online (http://clincancerres.aacrjournals.org/).

Requests for reprints: Andrew M. Evens, Division of Hematology/Oncology, 676 N. St. Clair, Suite 850, Chicago, IL 60611. Phone: 312-695-4537; E-mail: a-evens@northwestern.edu.

doi:10.1158/1078-0432.CCR-08-2365

Translational Relevance

Histone deacetylase (HDAC) inhibitors affect genes that result in growth inhibition, differentiation, and apoptosis of cancer cells. The HDAC inhibitor Zolinza (vorinostat) was recently approved by the Food and Drug Administration as monotherapy for relapsed/refractory cutaneous T-cell lymphoma. Further preclinical study and clinical application of new-generation HDAC inhibitors in other subtypes of lymphoma is warranted. In the present study, we investigated the apoptotic potential and related molecular mechanisms of the new HDAC inhibitor PCI-24781. We showed that PCI-24781, at clinically achievable concentrations, induced concentration-dependent apoptosis in several non-Hodgkin lymphoma cell lines, a Hodgkin lymphoma cell line, and in primary lymphoid leukemia (CLL/SLL) cells. Cell death was ROS- and caspase-dependent and was associated with activation of nuclear factor κB pathways. In addition, synergistic cell death was achieved when PCI-24781 was combined with the proteasome inhibitor bortezomib. These data support the clinical use of PCI-24781 as a single agent or combined with bortezomib for the treatment of patients with relapsed/refractory lymphoma.

carcinoma in phase I trials (12) and it is being evaluated in phase II trials in a variety of malignancies. We evaluated the cytotoxicity and the mechanisms of cell death using the HDAC inhibitor PCI-24781 in Hodgkin lymphoma and non-Hodgkin lymphoma cell lines and among primary CLL/SLL cells.

Bortezomib is a proteasome inhibitor that received Food and Drug Administration approval in the United States for relapsed multiple myeloma and more recently for relapsed mantle cell lymphoma, where cell death has been associated with increased ROS (13–15). Inhibition of proteasome activity by bortezomib results in stabilization of IκB with resultant nuclear factor κB (NF-κB) inhibition as well as stabilization of p53 and Bax, leading to apoptosis. In addition, *in vitro* studies in solid tumors and hematologic malignancies (multiple myeloma and leukemia) have shown synergy when bortezomib and HDAC inhibitors are combined (16–20). There is, however, little information on the activity and mechanism of this combination in lymphoma, with only one prior report in lymphoma (mantle cell) where an HDAC inhibitor has been tested in combination with bortezomib (18). We hypothesized that concomitant exposure of PCI-24781 and bortezomib might enhance apoptosis in other subtypes of lymphoma through ROS-related mechanisms.

We show here that the HDAC inhibitor PCI-24781 induced concentration-dependent apoptosis in Hodgkin lymphoma and non-Hodgkin lymphoma cells, which was dependent on caspase and ROS production. Further, PCI-24781 exhibited strong synergy when combined with bortezomib, inducing ROS-dependent apoptosis in all non-Hodgkin lymphoma cell lines. Cell death induced by PCI-24781, bortezomib, and the combination occurred through interacting mechanisms including down-regulation of oxidative stress response and proteasome/NF-κB pathways, which were likely responsible in part for the observed synergy in these lymphoma cells.

Materials and Methods

Cell lines and reagents. The L428 Hodgkin lymphoma cell line and the non-Hodgkin lymphoma cell lines Ramos (Burkitt lymphoma), HF1 (follicular lymphoma), and SUDHL4 (large B-cell lymphoma) were cultured in RPMI1640 (Invitrogen) with 10% fetal bovine serum, L-glutamine, and penicillin/streptomycin (Invitrogen). Cells were maintained at 37°C with 5% CO_2. Bortezomib was provided by Millennium Pharmaceuticals and PCI-24781 provided by Pharmacyclics Inc. Q-VD-OPh was used for pan-caspase inhibition (Calbiochem), 6-carboxy-2′7′-dichlorodihydrofluorscein (H_2DCF-DA) for ROS, JC-1 and valinomycin, (Molecular Probes) for mitochondrial membrane potential, and catalase was obtained from Sigma-Aldrich. Antibodies for caspase 8, caspase 9, caspase 3, acetyl histone H3 and H4, poly (ADP-ribose) polymerase (PARP; Cell Signaling), c-Myc (BD Pharmingen), cytochrome C, and p21 (Santa Cruz Biotech) were used to study cell death pathways. GAPDH (Millipore Corporation) was used as a loading control for Western blotting. Secondary antibodies included horseradish peroxidase–conjugated antirabbit and antimouse immunoglobulin antibodies (Santa Cruz Biotech). The AnnexinV-FITC detection kit (Biosource-Invitrogen) was used to measure apoptosis.

Primary lymphoid leukemia cells. Following informed consent, peripheral blood was drawn from four patients with primary lymphoid leukemia (CLL/SLL). Patient 1 was a 78-year-old man with newly diagnosed CLL/SLL [absolute lymphocyte count of 95.2 K/uL, hemoglobin 10.4 g/dL, no thrombocytopenia, presence of bulky (>7.5 cm) lymphadenopathy, with fluorescence *in situ* hybridization studies showing trisomy 12 in 48% of nuclei and a 13q deletion of both chromosomes 13 in 92% of nuclei]. Patients 2 and 3 were 46- and 68-year-old men with newly diagnosed CLL/SLL both with 11q deletion and both with absolute lymphocyte count of >75.0 K/uL without anemia or thrombocytopenia. Patient 4 was a 61-year-old female with relapsed CLL/SLL with 17p deletion with absolute lymphocyte count of 122.0 K/uL and platelets of 20.0 K/uL. All peripheral blood was diluted 1:1 with PBS (Ca^{2+} and Mg^{2+} free) and was layered on top of Ficoll-Paque Plus (Sigma). Samples were then centrifuged at 150 × *g* for 20 min at room temperature; the buffy coat layer was removed and centrifuged again. Isolated peripheral blood mononuclear cells were then resuspended in RPMI plus 10% fetal bovine serum to 1.5×10^6 cells/mL.

Quantification of apoptosis. All cell lines and CLL/SLL cells were incubated with PCI-24781 and/or bortezomib for 24 to 48 h. Cell viability was examined morphologically after staining with trypan blue and by analysis of apoptosis using fluorescence activated cell sorting (FACS) after staining with Annexin V-FITC and propidium iodide. In brief, after treatment, 1×10^6 cells were washed with PBS and then labeled with Annexin V-FITC/propidium iodide in the binding buffer according to the manufacturer's protocol. Fluorescent signals of FITC and propidium iodide were detected at 518 nm and 620 nm, respectively, on a Beckman Coulter FACS instrument. The data were analyzed with Flow Jo software (Tree Star). For each analysis 20,000 events were recorded.

Measurement of ROS. Intracellular ROS concentration was determined by using cell permeable dyes as described previously (21, 22). In brief, cells were washed with PBS and resuspended in 1 mL of RPMI containing 5 μmol/L H_2DCF-DA and incubated at 37°C for 30 min in the dark. ROS were measured by oxidation of H_2DCFDA to DCF. Fluorescence intensity was read by flow cytometry on the FL1 channel.

Western blot analysis. Cells were centrifuged, washed with cold PBS, and lysed on ice for 30 min in lysis buffer containing protease and phosphatase inhibitors. Protein concentrations were determined with the Bio-Rad protein assay kit (Bio-Rad). Total protein (50 μg) was electrophoresed on 12% SDS polyacrylamide gels and bands were visualized by chemiluminescence (Amersham Biosciences).

Measurement of mitochondrial membrane potential. Mitochondrial membrane potential (MMP) was measured by flow cytometry using JC-1 staining. Cells were washed with HBBS and incubated with 4 μg/mL JC-1 dye in HBSS for 15 min at 37°C in an incubator. Cells were washed with HBSS and immediately subjected to flow cytometric analysis.

Cell cycle analysis. Distinct phases of the cell cycle were distinguished by propidium iodide flow cytometry. Cells were washed in ice cold PBS, fixed in 70% ethanol, and stained for 30 min at 37°C with propidium iodide (50 μg/mL propidium iodide in hypotonic sodium citrate solution containing 50 μg/mL RNase) followed by flow cytometric analysis. The percentage of cells in G_1, S, and G_2/M phases were determined using the cell cycle analysis program Modfit LT (Verity Software).

Protein extracts and electrophoretic mobility shift assay. Electrophoretic mobility shift assay was done using a gel-shift kit from Panomics. In brief, cellular extracts were prepared as described earlier and protein concentrations were determined using Bio-Rad's protein assay reagent. The cellular extracts were then incubated with a biotin-labeled NF-κB probe for 30 min at 15°C. The extracts were electrophoresed on a 6% polyacrylamide gel and transferred to a Hybond nylon membrane (Pall Corporation). The membrane was blocked for 15 min in blocking buffer followed by 15 min incubation with streptavidin–horseradish peroxidase antibody in the blocking buffer. Membranes were washed three times, developed using the detection kit, and visualized using hyperfilm ECL (Amersham Biosciences).

Reverse transcription-PCR analysis. Taqman Gene Expression Assays for selected genes were obtained from Applied Biosystems Inc. One-step reverse transcription PCR (RT-PCR) was carried out in triplicate on 25 ng of total RNA from each sample on an ABI PRISM 7300 instrument according to the manufacturer's standard protocols. The mRNA levels for each gene were normalized to the amount of RNA in the well as measured in parallel using Ribogreen (Molecular Probes). The treated samples were then normalized to the vehicle control at that time point.

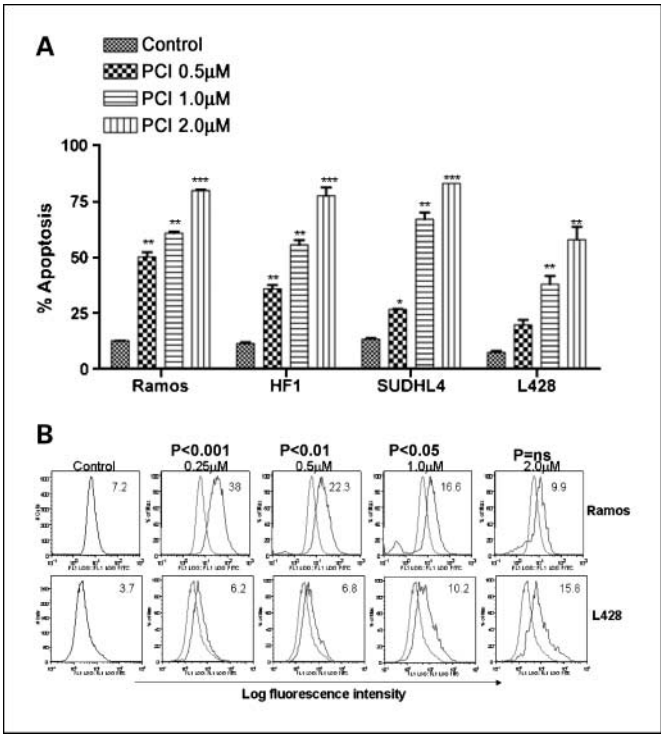

Fig. 1. PCI-24781 (PCI) concentration-dependent apoptosis in lymphoma cell lines. *A,* Ramos, HF1, SUDHL4, and L428 lymphoma cell lines were cultured with increasing concentrations (0.5-2.0 μmol/L) of PCI-24781 for 48 h. Percentage apoptosis was measured by Annexin V/propidium iodide staining and analyzed by flow cytometry. *B,* Ramos and L428 cell lines were cultured with indicated concentrations of PCI-24781 for 24 h and ROS was measured. At each concentration, histograms on the left denote control, whereas histograms on the right denote treatment with PCI-24781. Peak shift to right represents an increase in ROS production. $*P < 0.05$, $**P < 0.01$, and $***P < 0.001$ compared with control (RPMI).

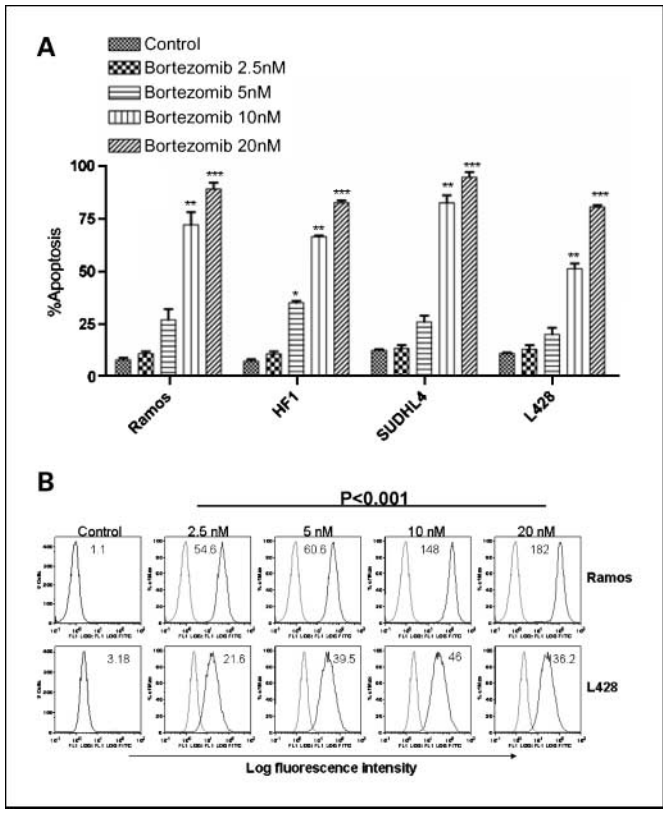

Fig. 2. Bortezomib in lymphoma cell lines. *A,* bortezomib induced concentration-dependent apoptosis in Ramos, HF1, SUDHL-4, and L-428. Cells were treated with indicated increasing concentrations of bortezomib, and at 48 h the percentage of apoptotic cells was determined by Annexin V/propidium iodide staining and measured by flow cytometry. *B,* ROS levels were measured by flow cytometry in Ramos and L428 cells following incubation of cells with bortezomib for 6 h followed by staining with H_2DCF-DA. At each concentration, histograms on the left denote control, whereas histograms on the right denote treatment with bortezomib. Peak shift to right represents an increase in ROS production. $*P < 0.05$ and $**P < 0.01$ compared with control (RPMI).

Gene expression profiling. The RNA expression profile was analyzed on custom Codelink oligonucleotide arrays (GE Biosciences), each containing 1857 gene probes, representing cellular cancer-related pathways, selected from the Codelink Human Genome arrays used in previous work (11, 23). cRNA probes were prepared from the total RNA isolated from treated and control cells, and hybridized to the arrays using standard protocols (Codelink Protocol v2.1). Arrays were hybridized for 18 h at 37°C, washed, and detected with Strepatavidin-Alexa 647. They were scanned with a GenePix 4000B scanner (Molecular Devices) and the images were processed with Codelink 4.0 Batch Processing software. The data were then analyzed in Genespring (Agilent Inc.); only genes passing quality filters ("G") and *P* value cutoff of 0.05 were used in the analyses.

Statistics. For all apoptosis experiments (Annexin V/propidium iodide and MMP), values represent the mean from three independent studies done in triplicate. Differences in groups were assessed by Student's *t* test and were considered statistically significant at $P < 0.05$, < 0.01, and < 0.001. For the experiments combining bortezomib and PCI-24781, synergy was determined using isobologram analysis based on the method of Chou and Talay using the Calcusyn (Biosoft) software program (24). This method is based on the equation: CI = (D)

1/(Dx)1+(D)2/(Dx)2, where CI is the combination index, D1 and D2 are concentrations of drug 1 and drug 2 that have x effect when used in combination, and (Dx)1 and (Dx)2 are the concentrations of drug 1 and drug 2 that have the same x effect when used alone.

Results

PCI-24781 time- and concentration-dependent apoptosis in Hodgkin lymphoma and non-Hodgkin lymphoma cell lines. The four lymphoma cell lines were exposed to increasing concentrations (0.5-2 μmol/L) of PCI-24781 for 48 hours. PCI-24781 induced apoptosis in all cell lines in a concentration-dependent manner (Fig. 1A). The IC_{50} of PCI-24781 was 0.5 μmol/L for Ramos, 0.8 μmol/L for SUDHL4, 0.9 μmol/L for HF1, and 1.4μmol/L for L428. Apoptosis was also time-dependent, with increasing cell death from 24 through 72 hours (data not shown). Several reports have indicated that the activity of HDAC inhibitors occur through production of ROS (5, 7–9). A 3-fold increase in ROS was seen here in Ramos and L428 cells following 24-hour exposure of PCI-24781 (Fig. 1B). Similar ROS production was also shown in SUDHL4 and HF1 cells (data not shown).

Bortezomib concentration-dependent apoptosis. Concentration-dependent apoptosis was seen in all lymphoma cell lines following 48-hour exposure with increasing concentrations of bortezomib (Fig. 2A). The IC_{50} for bortezomib was 20 nmol/L for L428 and 10 nmol/L for all three non-Hodgkin lymphoma cell lines. We next investigated whether apoptosis induced by bortezomib was associated with ROS production. As shown in Fig. 2B, treatment of cells with bortezomib resulted in >10-fold increase in ROS in a concentration-dependent manner in Ramos and L428 cells.

PCI-24781 combined with bortezomib. At 48 hours, all cell lines exhibited a significant increase in apoptosis with the combined PCI-24781/bortezomib as shown in Fig. 3A. Combined treatment with 0.5 μmol/L PCI-24781 and 5 nmol/L bortezomib resulted in synergistic apoptosis in all three non-Hodgkin lymphoma cell lines, whereas the effects were additive or synergistic depending on concentrations of the drugs used in the L428 Hodgkin lymphoma cell line (Figs. 3A and Supplemental Fig. S1). As shown by isobologram (Fig. 3B), Ramos cells displayed stronger synergy (CI = 0.19 for 0.5 μmol/L PCI-24781 and 5 nmol/L bortezomib) compared with other cell lines (CI = 0.3 to 0.6). In L428 cells, combination index values indicated synergy with 10 nmol/L bortezomib and 1 μmol/L PCI-24781 (CI = 0.6), whereas 5 nmol/L bortezomib and 0.5 μmol/L PCI-24781 was additive (CI of 1.1; data not shown). An increase in ROS was also observed with the combination of PCI-24781/bortezomib in Ramos as shown in Fig. 3C. Cells were coincubated with catalase, a free radical scavenger that degrades hydrogen peroxide. In Ramos (Fig. 3D) and L428 (Fig. 3E), apoptosis induced by PCI-24781, bortezomib, and PCI-24781/bortezomib combination were all blocked in the presence of catalase, suggesting that the effects on apoptosis are in part ROS-mediated (Fig. 3D and E). A similar effect of abrogated apoptosis by catalase was observed in HF1 and SUDHL4 cells (Supplemental Fig. S2). Primary CLL/SLL cells were exposed to increasing concentrations (0.125-2.0 μmol/L) of PCI-24781 for 48 hours. PCI-24781 induced concentration-dependent apoptosis with an associated IC_{50} of 0.5 μmol/L in CLL/SLL primary cells. Bortezomib alone also induced apoptosis at 5 nmol/L, whereas the combination of PCI-24781 and bortezomib resulted in additive cell death (Fig. 3F).

PCI-24781/bortezomib-induced apoptosis is associated with early mitochondrial events ($\Delta\Psi_m$), caspase activation, and PARP cleavage. Mitochondria play a crucial role in the regulation of programmed cell death (25). The release of proteins from the intermembrane space of mitochondria is a pivotal event in the initiation of the intrinsic cascade of apoptosis (26). Ramos cells showed 60% loss of MMP ($\Delta\Psi_m$) with 5 nmol/L bortezomib and <20% with 2.5 nmol/L (Fig. 4A), whereas PCI-24781 alone showed 25% to 30% $\Delta\Psi_m$ (0.5-1 μmol/L). However, the combination of bortezomib (2.5 nmol/L) and PCI-24781 (0.5 μmol/L) resulted in >80% $\Delta\Psi_m$ ($P < 0.01$ combination versus single agents). L428 cells showed minimal $\Delta\Psi_m$ following bortezomib treatment, whereas 50% to 60% $\Delta\Psi_m$ was observed with PCI-24781 alone (Fig. 4B). Higher concentrations of PCI-24781 alone were needed in L428 compared with Ramos, whereas the combination resulted in >75% $\Delta\Psi_m$. Similar loss of MMP after treatment of cells with bortezomib and PCI-24781 alone or with the combination was also observed in HF1 and SUDHL4 cells (Supplemental Fig. S3).

The involvement of caspases in PCI-24781 and bortezomib-induced apoptosis was assessed by assessment of cleaved caspases and PARP by Western blotting. As shown in Fig. 4C, both agents induced caspase 8 and 9 cleavage when used alone, whereas the combination of bortezomib and PCI-24781 resulted in markedly increased cleaved caspase 8 and caspase 9 compared with either agent alone (Fig. 4C). Cleavage of caspase 3 and PARP was also observed following treatment of cells with bortezomib or PCI-24781. Activation of caspases and PARP was also observed in HF1 and SUDHL4 cells (Supplemental Fig. S4) following treatment with bortezomib and PCI combination. To assess the importance of caspase activation in bortezomib and/or PCI-24781-induced cell death, cells were coincubated with the broad-spectrum caspase inhibitor, Q-VD-OPh. Figure 4D shows that PCI-24781/bortezomib-induced cell death in L428 and Ramos cells was in part caspase-dependent. Inhibition of apoptosis with the pan-caspase inhibitor was also observed in HF1 and SUDHL4 cells (Supplemental Fig. S5).

Apoptosis is associated with cell cycle arrest and p21 up-regulation. Concentration-dependent G_2/M arrest occurred following treatment of Ramos and L428 cells with bortezomib (Fig. 5A and B) that was accompanied by a decreased number of cells within the S and G_1 phases. Treatment with PCI-24781 resulted in G_0/G_1 arrest with a decrease in G_2/M and S phase cell population in both Ramos and L428 (Fig. 5A and B). HF1 and SUDHL4 cells also showed G_0/G_1 arrest following treatment of cells with PCI -24781 (Supplemental Fig. S6). The combination of bortezomib and PCI-24781 was similar to the effect of bortezomib or PCI-24781, although PCI-24781 alone resulted in >75% G_0/G_1 arrest. The biological effects of HDAC inhibitors are thought to be related in part by modifications of the acetylation state of histones. Hyperacetylation of histone H3 and H4 was observed following PCI-24781 treatment (Fig. 5C). Interestingly, bortezomib also provoked a small increase in the acetylation of histone H4, although to a lesser extent. However, the combination of PCI-24781 and bortezomib resulted in a significant increase in histone acetylation (Fig. 5C). Transcription of the CDK inhibitor p21 (CDKN1A) is regulated in part by histone acetylation status (27), and up-regulation of p21 has been reported with HDAC inhibitors (28, 29).

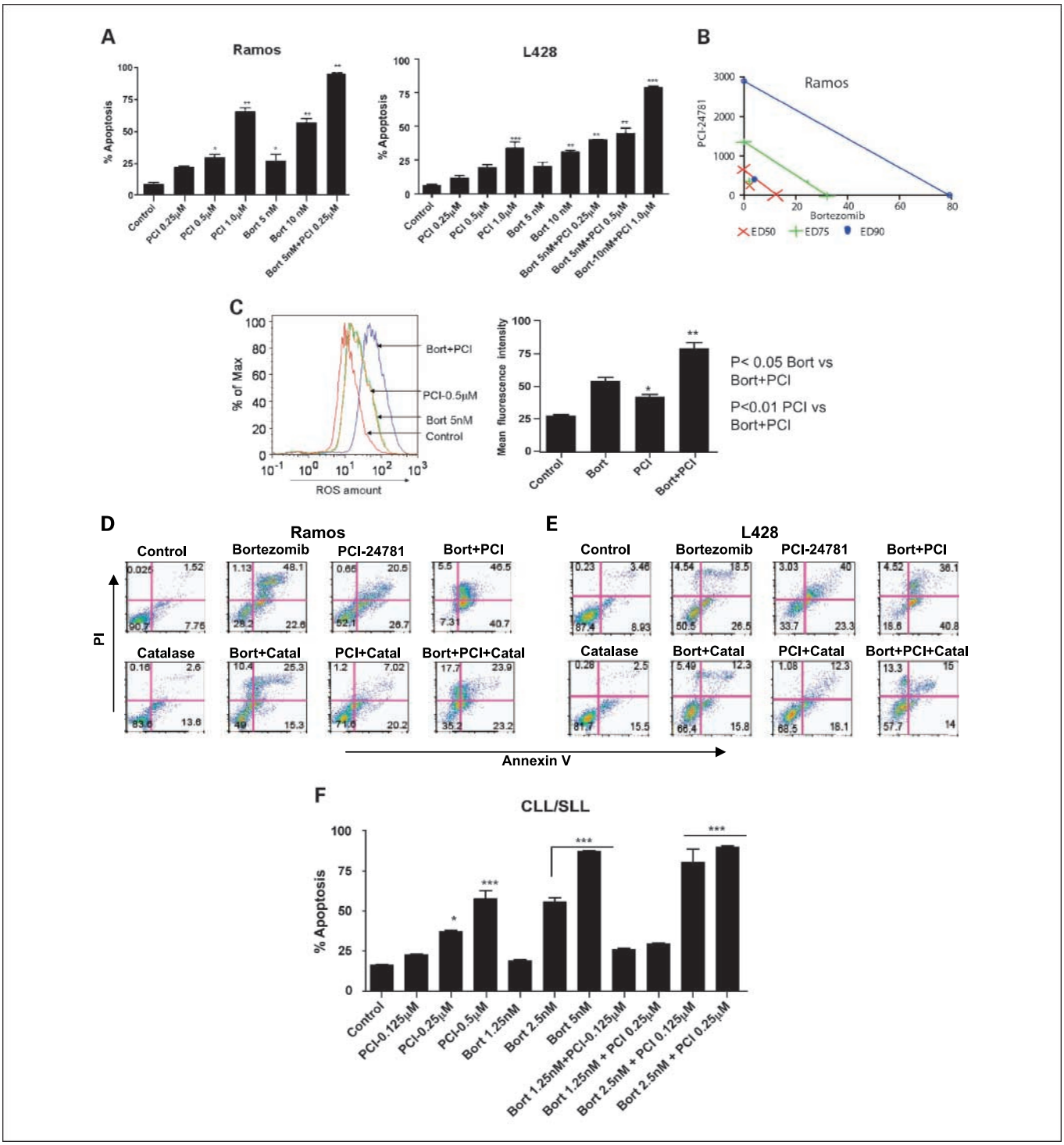

Fig. 3. Combined PCI-24781 with bortezomib induced synergistic apoptosis that was ROS-dependent. *A,* cotreatment with bortezomib enhanced PCI-24781-related apoptosis. Ramos and L428 cell lines were treated with varying concentrations of PCI-24781 (0.25-0.5 μmol/L) and bortezomib (5-10 nmol/L) either alone or in combination as indicated for 48 h. Percentage of apoptotic cells was measured by flow cytometry after Annexin V/propidium iodide staining. *B,* isobolograms of the Ramos cell line treated with both PCI-24781 and bortezomib. Data points (*blue circle, green plus, red x*) indicate specific PCI-24781 and bortezomib concentrations at which apoptosis was 50%, 75%, or 90% as indicated, after 48 h. Lines connecting cytotoxic IC_{50}, IC_{75}, or IC_{90} for each drug signify a linear relationship between the drugs. Data points below each respective straight colored line indicate synergistic cytotoxicity. *C,* ROS production in Ramos. Ramos cells were treated with the indicated concentrations of bortezomib and PCI-24781 for 4 h followed by staining with H_2DCF-DA analyzed by flow cytometry. Red line, no drug treatment; blue line, with bortezomib; green line, with PCI-24781; yellow line, bortezomib/PCI-24781 combined. Apoptosis in Ramos (*D*) and L-428 (*E*) was ROS-dependent. Catalase inhibited bortezomib and PCI-24781-induced apoptosis in Ramos and L428. Cell lines were treated with 4,000 units of catalase for 2 h following incubation with the 10 nmol/L bortezomib or 0.5 μmol/L (Ramos)/1.0 μmol/L (L428) PCI-24781 or combination bortezomib/PCI (Ramos 5 nmol/L bortezomib plus 0.5 μmol/L PCI and L428 with 10 nmol/L bortezomib plus 1 μmol/L PCI) for 48 h. *F,* apoptosis in primary CLL/SLL cells. For all experiments, the percentage of apoptotic cells was determined by Annexin V/propidium iodide staining followed by flow cytometric analysis. $*P < 0.05$, $**P < 0.01$, and $***P < 0.001$. Unless designated, *P* values for single-agents reflect bortezomib or PCI-24781 versus control; *P* values for combinations reflect bortezomib/PCI-24781 versus matching single-agent concentrations.

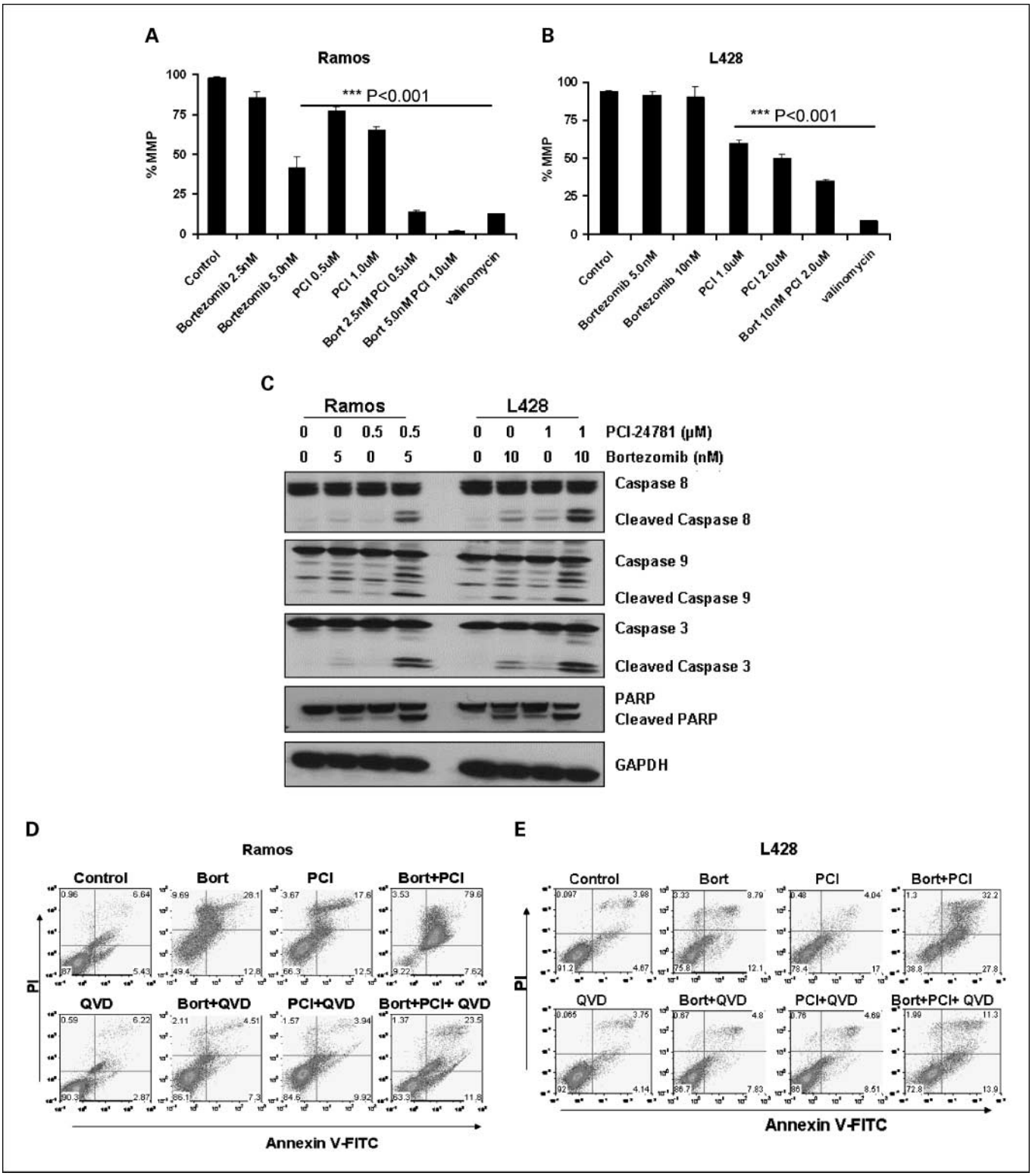

Fig. 4. $\Delta\Psi_m$ and caspase-dependent apoptosis with PCI-24781 and/or bortezomib. Ramos (*A*) and L428 (*B*) cells were treated with indicated concentrations of bortezomib and PCI-24781 for 24 h. The percentage of cells exhibiting loss of mitochondrial membrane potential ($\Delta\Psi_m$) was determined by JC-1 staining followed by flow cytometric analysis. *C*, Western blot analysis of cleaved caspases 3, 9, 8, and PARP activation in Ramos and L428 cells. Cells were treated with the indicated concentrations of bortezomib or PCI-24781 for 24 h. The pan-caspase inhibitor Q-VD-OPh, inhibited bortezomib/PCI-24781-induced apoptosis in Ramos (*D*) and (*E*) L428 cells. Ramos and L428 cells were treated with either 5 nmol/L (Ramos) and 10 nmol/L (L428) bortezomib or 0.5 μmol/L (Ramos) and 1.0 μmol/L (L428) PCI or combined bortezomib/PCI-24781 (5 nmol/L bortezomib and 0.5 μmol/L PCI-24781 in Ramos and 10 nmol/L bortezomib and 1 μmol/L PCI-24781 in L428). For 48 h alone (control) or with 4-h pretreatment with 50 μmol/L Q-VD-OPh. Apoptotic cells were detected by Annexin V/propidium iodide staining and measured by flow cytometry. $^*P < 0.05$, $^{**}P < 0.01$, and $^{***}P < 0.001$. Unless designated, *P* values for single agents reflect bortezomib or PCI-24781 versus control; *P* values for combinations reflect bortezomib/PCI-24781 versus matching single-agent concentrations. Bort, bortezomib. MMP, mitochondrial membrane potential; ns, not significant; QVD, Q-VD-OPh.

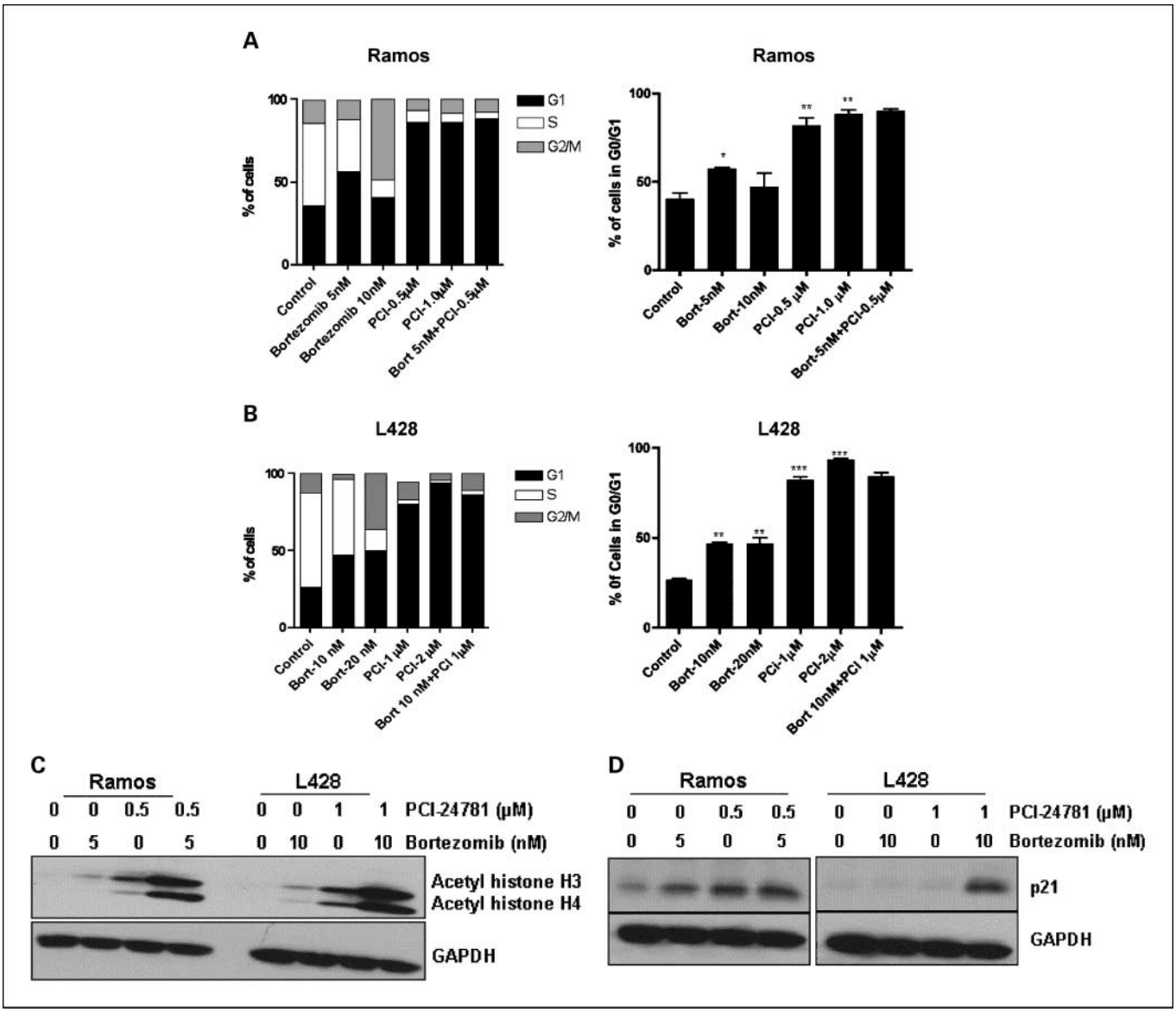

Fig. 5. Bortezomib and PCI-24781 cell cycle arrest and histone acetylation. Ramos (*A*) and L428 (*B*) cells were treated with the indicated concentrations of bortezomib or PCI-24781 and the combination for 24 h and then stained with propidium iodide and their cell cycle profiles were examined. On the right side is the comparison of G1 fraction in all the population. *C*, Western blot showing histone hyperacetylation and p21 up-regulation (*D*). Cells were treated with 5 nmol/L (Ramos) or 10 nmol/L (L428) of bortezomib and 0.5 μmol/L (Ramos) or 1.0 μmol/L (L428) of PCI-24781 for 16 h. *D*, the level of acetyl histone H3/H4 and p21 protein was measured using antibody as described in the Methods. GAPDH was used as internal control for all Western blots. $*P < 0.05$, $**P < 0.01$, and $***P < 0.001$. *P* values for single-agents reflect bortezomib or PCI-24781 versus control. Combination bortezomib/PCI-24781 versus single-agents was not significant.

We observed increased protein levels of p21 with PCI-24781, and more so with the combination (Fig. 5D). A significant increase in histone H3 acetylation was observed in HF1 and SUDHL4 cells. p21 was also up-regulated in HFI and SUDHL4 following treatment with the combination of bortezomib and PCI-24781 (Supplemental Fig. S7).

Gene expression profiling following PCI-24781 and/or bortezomib. Gene expression profiling using the pathway analysis chip revealed a subset of genes whose expression was altered in response to 0.25 μmol/L PCI-24781 and/or 3 nmol/L bortezomib in Ramos cells. These concentrations were chosen because higher concentrations led to increased cell death at the 24-hour time point. The Codelink oligonucleotide microarray used also included genes in other pathways of interest, including those previously shown to be affected by PCI-24781 treatment (11). Statistical analyses of the data revealed a coefficient of variation of 11.52% between four replicates, leading to a minimum detectable fold change of 1.3 according to the Codelink Analysis software (data not shown). Selected genes meeting the *P*-value cutoff of 0.05 are shown in Table 1.

The classical targets of both drugs were affected, including proteasome components and several HDACs (HDACs 1, 2, 7, 8) with bortezomib and PCI-24781 treatment, respectively. In

Table 1. Selected genes from expression analysis following 24-h treatment with PCI-24781, bortezomib, or the combination (in Ramos cells)

Accn #	Up-regulated genes	0.25 μmol/L PCI/3 nmol/L Bor		
	Name	PCI-24781	Bortezomib	Combination*
Cell cycle–related				
NM_000075	Cyclin-dependent kinase 4 (CDK4)	0.49	0.83	0.37
NM_001237	Cyclin A2 (CCNA2)	0.43	0.87	0.37
NM_001950	E2F transcription factor 4, p107/p130-binding (E2F4)	0.48	0.79	0.40
NM_001951	E2F transcription factor 5, p130-binding (E2F5)	0.46	0.98	0.43
NM_003903	CDC16 cell division cycle 16 homolog (S cerevisiae) (CDC16)	0.61	0.78	0.43
NM_031966	Cyclin B1 (CCNB1)	0.55	0.90	0.43
NM_001760	Cyclin D3 (CCND3)	0.48	1.02	0.46
NM_001255	CDC20 cell division cycle 20 homolog (S cerevisiae; CDC20)	0.61	0.82	0.46
NM_001262	Cyclin-dependent kinase inhibitor 2C (p18, inhibits CDK4; CDKN2C)	0.61	1.15	0.56
NM_001238	Cyclin E1 (CCNE1)	0.56	1.05	0.60
NM_001239	Cyclin H (CCNH)	0.74	0.90	0.64
NM_004701	Cyclin B2 (CCNB2)	0.90	0.95	0.67
NM_001240	Cyclin T1 (CCNT1)	0.67	1.16	0.71
NM_001761	Cyclin F (CCNF)	0.77	0.93	0.74
NM_001258	Cyclin-dependent kinase 3 (CDK3)	0.60	1.14	0.80
NM_004702	Cyclin E2 (CCNE2)	0.76	1.40	0.82
NM_001759	Cyclin D2 (CCND2)	0.85	0.87	0.86
Proteasome				
NM_017518	26S proteasome-associated UCH interacting protein 1 (UIP1)	0.36	0.79	0.29
NM_002811	Proteasome 26S subunit, non-ATPase, 7 (PSMD7)	0.68	1.44	0.57
NM_005047	Proteasome 26S subunit, non-ATPase, 5 (PSMD5)	0.61	1.04	0.70
NM_002812	Proteasome 26S subunit, non-ATPase, 8 (PSMD8)	0.60	1.13	0.70
NM_002794	Proteasome subunit, beta type, 2 (PSMB2)	0.75	1.26	0.83
NM_002790	Proteasome subunit, alpha type, 5 (PSMA5)	0.74	1.43	0.92
Oxidative stress				
NM_006440	Thioredoxin reductase 2 (TXNRD2)	0.36	0.83	0.24
NM_145177	Dehydrogenase/reductase (SDR family) X-linked (DHRSX)	0.37	0.87	0.40
NM_012473	Thioredoxin 2 (TXN2)	0.60	0.94	0.53
NM_145792	Microsomal glutathione S-transferase 1 (MGST1)	0.66	0.83	0.54
NM_002134	Heme oxygenase (decycling) 2 (HMOX2)	0.66	0.89	0.57
NM_012331	Methionine sulfoxide reductase A (MSRA)	0.74	0.86	0.72
NM_000637	Glutathione reductase (GSR)	0.61	1.46	0.80
NM_001752	Catalase (CAT)	0.93	0.72	0.83
NM_147149	Glutathione S-transferase M4 (GSTM4)	0.89	0.92	0.87
NM_182743	Thioredoxin reductase 1 (TXNRD1)	0.81	1.69	0.98
HDACs and histones				
NM_016596	Histone deacetylase 7A (HDAC7A)	0.35	1.06	0.31
NM_004964	Histone deacetylase 1 (HDAC1)	0.74	0.89	0.55
NM_018486	Histone deacetylase 8 (HDAC8)	0.76	1.02	0.64
NM_001527	Histone deacetylase 2 (HDAC2)	0.94	0.97	0.87
NF-kB target genes				
BC022556	Myc target 1 (MYCT1)	0.12	0.92	0.08
NM_001556	IkB kinase beta (IKBKB)	0.60	1.13	0.32
NM_032778	MYC induced nuclear antigen (MINA)	0.40	0.87	0.33
NM_002983	Chemokine (C-C motif) ligand 3 (CCL3)	0.46	0.85	0.42
NM_003998	NF-kB p105 (NFKB1)	0.47	1.19	0.43
NM_002467	v-myc viral oncogene homolog (MYC)	0.80	0.95	0.67
NM_006273	Chemokine (C-C motif) ligand 7 (CCL7)	0.51	0.61	0.69
NM_006509	Rel B, NFkB subunit (RELB)	0.32	1.27	0.72
NM_014002	IkB kinase ε (IKBKE)	0.59	0.88	0.76
NM_000600	Interleukin 6 (interferon, ρ 2) (IL6)	0.84	1.28	0.81
NM_002503	IkB ρ (NFKBIB)	0.80	1.22	0.82
BC033522	Rel A, NFkB p65 subunit	0.92	1.04	0.85
Apoptosis				
NM_001168	Baculoviral IAP repeat-containing 5 (surviving; BIRC5)	0.56	0.83	0.54
NM_003879	CASP8 and FADD-like apoptosis regulator (CFLAR; c-FLIP)	0.60	1.03	0.56
NM_016252	Baculoviral IAP repeat-containing 6 (apollon; BIRC6)	0.75	1.10	0.72

(*Continued to the following page*)

addition, significant down-regulation of genes in several pathways including cell cycle, proteasome, oxidative stress, and apoptosis were observed in response to PCI-24781 alone; these effects were enhanced in combination with bortezomib. In particular, it was observed that several antioxidant genes were down-regulated by PCI-24781 alone and in combination

Table 1. Selected genes from expression analysis following 24-h treatment with PCI-24781, bortezomib, or the combination (in Ramos cells) (Cont'd)

Accn #	Up-regulated genes	0.25 μmol/L PCI/3 nmol/L Bor		
	Name	PCI-24781	Bortezomib	Combination*
Apoptosis and tumor necrosis factor receptor related				
NM_000177	Gelsolin (GSN)	6.99	1.04	7.56
NM_032974	Caspase 10, apoptosis-related cysteine protease (CASP10)	7.99	0.81	6.16
NM_006573	Tumor necrosis factor (ligand) superfamily, member 13b (TNFSF13B)	3.59	1.91	3.38
NM_016639	Tumor necrosis factor receptor superfamily, member 12A (TNFRSF12A)	2.02	0.79	2.44
NM_018647	Tumor necrosis factor receptor superfamily, member 19 (TNFRSF19)	−0.11	1.85	2.23
NM_003842	Tumor necrosis factor receptor superfamily, member 10b (TNFRSF10B)	2.61	1.15	2.22
NM_014417	BCL2 binding component 3 (BBC3; PUMA)	0.95	1.69	1.85
NM_138621	BCL2-like 11 (apoptosis facilitator) (BCL2L11)	1.43	0.94	1.79
NM_000043	Fas (TNFRSF6; FAS)	1.72	1.46	1.73
NM_006290	Tumor necrosis factor, α-induced protein 3 (TNFAIP3)	1.35	0.95	1.69
NM_003300	TNF receptor-associated factor 3 (TRAF3)	2.80	0.78	1.62
NM_000594	Tumor necrosis factor (TNF superfamily, member 2; TNF)	0.99	0.94	1.31
Cell cycle inhibitors				
NM_000389	Cyclin-dependent kinase inhibitor 1A (p21, Cip1; CDKN1A)	25.87	0.92	28.45
NM_000076	Cyclin-dependent kinase inhibitor 1C (p57, Kip2; CDKN1C)	6.21	0.46	16.18
L36844	p15INK4B CDK inhibitory protein (CDKN2B)	5.26	2.54	4.49
NM_004064	Cyclin-dependent kinase inhibitor 1B (p27, Kip1; CDKN1B)	4.34	2.15	3.51
Cytoskeletal				
NM_178012	Tubulin, β 2B (TUBB2B)	14.66	0.87	16.45
BC056264	Histone 1, H2bg (HIST1H2BF)	6.42	1.17	5.65
NM_021052	Histone 1, H2ae (HIST1H2AE)	2.23	0.91	3.76
NM_021065	Histone 1, H2ad (HIST1H2AD)	1.47	0.69	2.69
NM_003543	Histone 1, H4h (HIST1H4H)	1.01	1.20	1.88
NM_001015053	Histone deacetylase 5 (HDAC5)	1.22	1.09	1.71
NM_003509	Histone 1, H2ai (HIST1H2AI)	1.12	0.80	1.45
NM_003516	Histone 2, H2aa (HIST2H2AA)	1.13	1.00	1.41
NM_003528	Histone 2, H2be (HIST2H2BE)	2.11	0.84	1.23
Oxidative stress				
NM_002738	Protein kinase C, β1 (PRKCB1)	14.00	0.86	11.85
NM_002133	Heme oxygenase (decycling) 1 (HMOX1)	6.52	1.82	7.53
NM_004417	Dual specificity phosphatase 1 (DUSP1)	3.49	0.67	5.54
NM_005346	Heat shock 70kDa protein 1B (HSPA1B)	2.23	3.74	5.27
Other				
NM_002206	Integrin, α7 (ITGA7)	15.21	1.47	15.01
NM_002228	v-jun sarcoma virus 17 oncogene homolog (JUN)	4.06	0.94	12.14
NM_000584	Interleukin 8 (IL8)	3.18	1.88	6.41
NM_000582	Osteopontin, early T-lymphocyte activation 1 (SPP1)	3.67	0.82	5.07
NM_004862	Lipopolysaccharide-induced TNF factor (LITAF)	2.26	1.20	2.08

NOTE: Changes are expressed as ratios of treated to control cell levels.
*Combination of PCI-24781 and bortezomib (0.25 μmol/L and 3 nmol/L, respectively).

with bortezomib, including thioredoxin-2 and thioredoxin reductase-2, heme oxygenase 2, catalase, glutathione reductase, and several glutathione reductases (Table 1). Some of these pathways have been previously linked to induction of apoptosis by these compounds. A marker for ROS induction, heme oxygenase 1 (*HMOX-1*), was also increased, but unlike HMOX-2, this gene may serve to facilitate apoptosis. It is likely that transcriptional control of these antioxidant genes by PCI-24781 enhances the ROS accumulation and ROS-dependent apoptosis observed in combination with bortezomib.

Interestingly, PCI-24781 seemed to induce down-regulation of the proteasome complex and many NF-κB target genes of both the canonical and alternative pathways [i.e., c-Myc, IκB-kinase (IKK)-β, NFkB1, and Rel B] as well as related chemokines and cytokines (including CCL3, CCL7, and IL-6). Several of these genes were further down-regulated by PCI-24781/bortezomib combination (c-Myc, *myc*-regulated genes, and the IKK catalytic subunits) supporting the mechanism of proteasome and NF-κB inhibition for synergy of this combination. Expression of the noncanonical (alternative) pathway components, NF-κB–inducing kinase (NIK), and the NF-κB subunit p52 were not affected by PCI-24781 and/or bortezomib (data not shown). Large increases were also observed in the levels of CDK inhibitors, including p21, consistent with the results shown before.

Inhibition of NF-κB. We measured the changes in mRNA and protein levels of several NF-κB targets. Accordingly, quantitative RT-PCR analysis of known NF-κB targets including NFκB1 (p105, the precursor of the NF-κB subunit p50), c-Myc, and the two IKK catalytic subunits IKKα (IKK1) and IKKβ (IKK2) were measured. PCI-24781 alone markedly decreased NF-κB1, and to a lesser extent c-Myc and IKKβ in Ramos cells (Fig. 6A). A significant decrease in the mRNA levels of NF-κB1, c-Myc, and IKK, following exposure to

bortezomib or PCI-24781 or the combination was observed in L428 cells (Supplemental Fig. S8). Moreover, a notable decrease in all four of these transcripts was seen with PCI-24781/bortezomib in combination. Finally, we analyzed the NF-κB subunit p65 (Rel A) and c-Myc protein levels in response to bortezomib and PCI-24781 alone and in combination, by Western blotting (Fig. 6B). NF-κB p65 protein levels did not change significantly, consistent with the gene expression results, whereas c-Myc protein was decreased by PCI-24781 alone and PCI-24781/bortezomib. A similar effect of bortezomib and PCI-24781 was also observed in HF1 and SUDHL4 cells (Supplemental Fig. S9). To further determine the effect that combined exposure of bortezomib and PCI-24781 has on NF-κB DNA-binding activity, electrophoretic mobility shift assay was done (Fig. 6C). A decrease in NF-κB activity was observed with 10 to 20 nmol/L bortezomib and 1 to 2 μmol/L PCI-24781 alone and in combination in Ramos and L428 cells. These findings support the concept that NF-κB signaling is a key component in the cell death pathways induced by PCI-24781 alone and in combination with bortezomib.

Discussion

We show that the broad-spectrum hydroxamic acid-based HDAC inhibitor PCI-24781 induced time- and concentration-dependent apoptosis in a Hodgkin lymphoma cell line, several non-Hodgkin lymphoma cell lines, and in primary CLL/SLL cells. PCI-24781 had an IC_{50} of <1 μmol/L in the non-Hodgkin lymphoma lines and <1.5 μmol/L for L428 cells, both clinically achievable concentrations (10). Apoptosis occurred through $\Delta\Psi_m$, ROS generation, and caspase activation in all cell lines. We observed that PCI-24781 alone induced a 3-fold increase in ROS. Furthermore, apoptosis induced by PCI-24781 was ROS-dependent, as cell death was abrogated when cells were pretreated with the antioxidant agent, catalase.

We also observed synergistic apoptosis in non-Hodgkin lymphoma cells when bortezomib was combined with PCI-24781. Combination studies of novel agents are important, in part to overcome clinical resistance to single-agent therapy in disease subsets where response is more limited, such as with bortezomib for diffuse large B-cell lymphoma (30) or Hodgkin lymphoma (31). Further, this work extends and

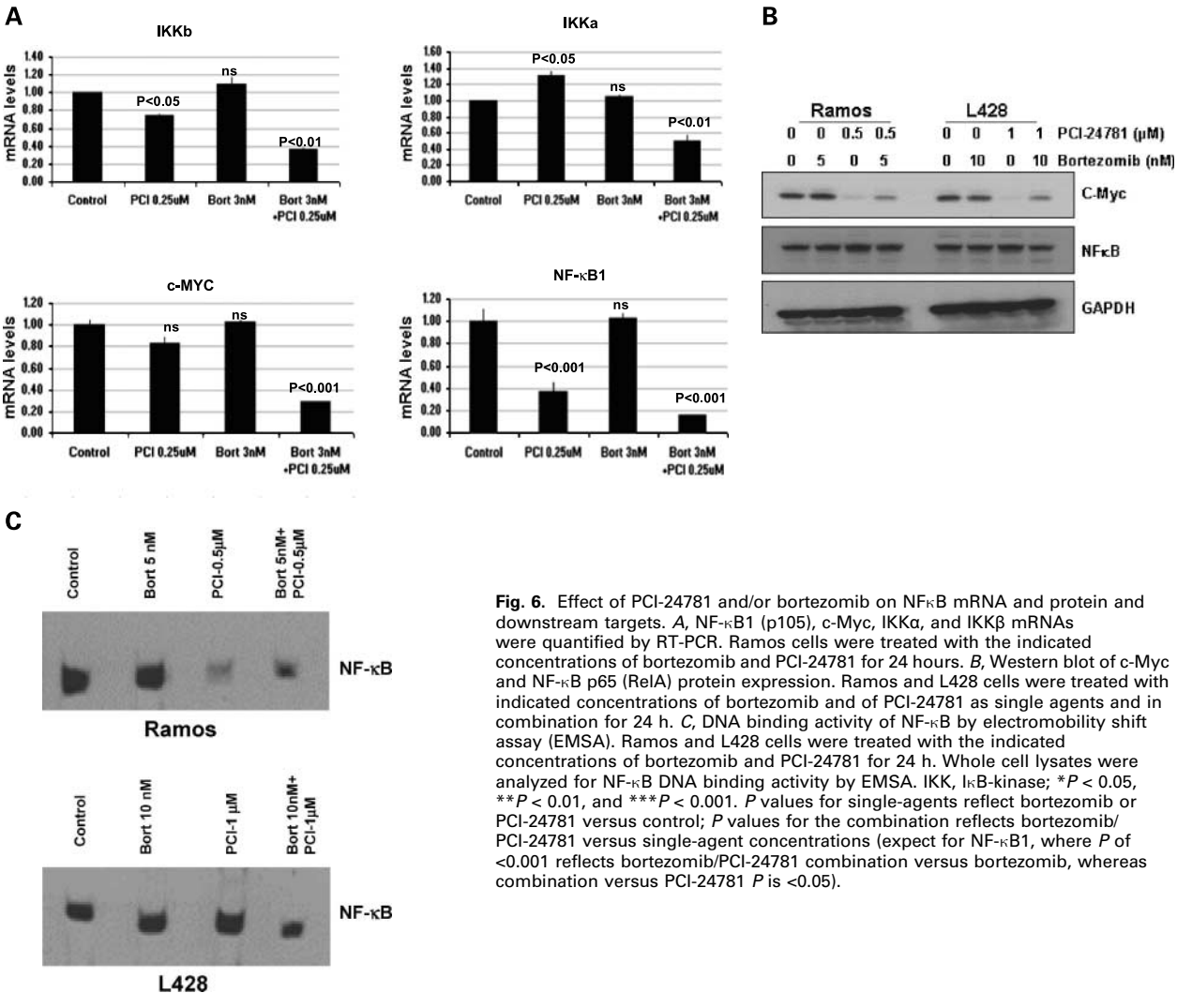

Fig. 6. Effect of PCI-24781 and/or bortezomib on NFκB mRNA and protein and downstream targets. *A*, NF-κB1 (p105), c-Myc, IKKα, and IKKβ mRNAs were quantified by RT-PCR. Ramos cells were treated with the indicated concentrations of bortezomib and PCI-24781 for 24 hours. *B*, Western blot of c-Myc and NF-κB p65 (RelA) protein expression. Ramos and L428 cells were treated with indicated concentrations of bortezomib and of PCI-24781 as single agents and in combination for 24 h. *C*, DNA binding activity of NF-κB by electromobility shift assay (EMSA). Ramos and L428 cells were treated with the indicated concentrations of bortezomib and PCI-24781 for 24 h. Whole cell lysates were analyzed for NF-κB DNA binding activity by EMSA. IKK, IκB-kinase; $*P < 0.05$, $**P < 0.01$, and $***P < 0.001$. *P* values for single-agents reflect bortezomib or PCI-24781 versus control; *P* values for the combination reflects bortezomib/PCI-24781 versus single-agent concentrations (expect for NF-κB1, where *P* of <0.001 reflects bortezomib/PCI-24781 combination versus bortezomib, whereas combination versus PCI-24781 *P* is <0.05).

offers mechanistic insights into the previous work in other tumor types regarding the ROS-dependent synergy between HDAC inhibitors and bortezomib (16–20). The mode of apoptosis induction by the PCI-24781/bortezomib combination involved activation of both extrinsic (caspase-8) and intrinsic (caspase-9) caspase pathways. Compared with either agent alone, PCI-24781 and bortezomib together led to highly increased levels of cleaved caspase-8, caspase-9, caspase-3, and PARP. The up-regulation of several members of the tumor necrosis factor receptor superfamily may lead to the activation of the extrinsic pathway, whereas the activation of the intrinsic pathway via caspase-9 is consistent with the relatively early $\Delta\Psi_m$ that is observed here. Moreover, cell death was caspase-dependent as shown with pan-caspase inhibition, which inhibited apoptosis induced by PCI-24781 alone and combined with bortezomib.

The activation of NF-κB is known to play a critical role in the oncogenesis of lymphoid malignancies (32, 33). Treatment with PCI-24781 alone led to down-regulation of several components of the proteasome complex as well as many NF-κB target genes, whereas the combination of PCI-24781 and bortezomib resulted in further down-regulation of several NF-κB target genes including c-Myc (at protein and mRNA levels), *myc*-regulated genes, as well as the two catalytic subunits of IKK (IKKα and IKKβ; Table 1 and Fig. 6A). More directly, the DNA-binding activity was also decreased following treatment of cells with these compounds as shown by the gel shift assay. The canonical NF-κB pathway seemed to be more dominant here as the PCI-24781/bortezomib combination primarily affected the p65/p50 complex through reduction of IKK activity and p50 expression (and its precursor, NF-κB1), which led to decreased nuclear translocation and decreased binding of NF-κB to its target promoters. HDAC inhibitors that increase acetylation of proteins require an intact NF-κB signaling pathway to induce cell cycle arrest in human myeloid leukemia cells (34).

We also present here the first reported gene expression profiling data using the combination of a HDAC inhibitor and bortezomib. A potential explanation of PCI-24781–induced cell death involves direct up-regulation of pro-oxidant genes (with resultant NF-κB inhibition and ROS production) and through the effects of direct inhibition of NF-κB and associated changes in antioxidant genes. Following PCI-24781 ± bortezomib, oxidative stress markers were up-regulated, whereas antioxidant genes were down-regulated. The oxidative stress marker HMOX-1, which was up-regulated in this study, can inhibit NF-κB activation by preventing its translocation into the nucleus and inhibiting the degradation of IκB (35, 36); indeed HMOX-1 has been shown to enhance bortezomib-induced cell death in leukemic cells (37). Further, we found that PCI-24781 down-regulated the expression of many antioxidant genes including *TXN2* and *TNXRD2*. Activation of NF-κB is known to play an important role in the oxidative stress response of tumor cells (38) in part through the regulation of antioxidant genes suggesting here that down-regulation of thioredoxin-2 and other anti-oxidant genes, inhibition of NF-κB, and induction of ROS could all act together to explain the mechanism of activity of PCI-24781 in lymphoma. It is also interesting that following PCI-24781 treatment, gene expression data showed down-regulation of c-FLIP and the pro-survival BIRC family members including survivin and apollon, which may all prevent cytochrome *c* release and caspase activation. Further studies are needed to confirm the detailed mechanism of caspase activation in response to PCI-24781 and/or bortezomib in lymphoma.

Finally, PCI-24781 mediated a prominent arrest of the lymphoma cells in the G_0/G_1 phase of the cell cycle, resulting in a marked decrease in S phase. Blockade of the cell cycle was accompanied by increased expression of p21, a cyclin-dependent kinase (CDK) inhibitor that plays an important role in cell cycle arrest during the G_1 or G_2 phase (39). Prominent increases were also observed in other CDK inhibitors, including CDKN1B, CDKN1C, and CDKN2B (Table 1). Concordant decreases in many cyclins and CDKs, most prominently CDK4 and cyclin A2, likely contributed to the dramatic increase in G_1 arrest and subsequent apoptosis in these lymphoma cell lines. As expected with a HDAC inhibitor, there was also an accumulation of acetylated histone H3 and H4 with PCI-24781 treatment in these cells, which was synergistically increased by adding bortezomib; however, we and others have shown that histone acetylation is not directly correlated with sensitivity (11, 40). It is likely, however, that the enhanced accumulation of p21 is due to increased histone acetylation in these cells (27). Further, histone acetylation (and its surrogate for compounds that inhibit HDAC6, tubulin acetylation) has proved to be an important and sensitive pharmacodynamic marker of HDAC activity in clinical studies, including the PCI-24781 studies currently underway.

In summary, our results show that the pan-HDAC inhibitor, PCI-24781, when used alone exhibited concentration-dependent apoptosis in a Hodgkin lymphoma cell line, several non-Hodgkin lymphoma cell lines, and primary CLL/SLL cells. Furthermore, the combination of PCI-24781 with bortezomib was strongly synergistic in all non-Hodgkin lymphoma cell lines. Apoptosis induced by PCI-24781 and by the combination were ROS- and caspase-dependent. Disruption of the cellular redox state with production of ROS and down-regulation of oxidative stress response genes may represent an important mechanism underlying lymphoma cell death in response to PCI-24781 ± bortezomib. We showed that the NF-κB pathway, which is a major regulator of the oxidative stress response in cells, was inhibited by PCI-24781 and further when combined with bortezomib. Finally, we showed that acetylation of histones and reexpression of p21 was greatly enhanced when bortezomib was added to PCI-24781. Thus, the combination of PCI-24781/bortezomib triggered cell death through interacting mechanisms including ROS generation, mitochondrial disruption, proteasome and NF-κB inhibition, cell cycle arrest, and caspase activation. Taken together our data suggest that PCI-24781 has potential therapeutic value in Hodgkin lymphoma and non-Hodgkin lymphoma as a single agent and in combination with bortezomib.

Disclosure of Potential Conflicts of Interest

A.M. Evens, Advisory Board, Millennium.

Acknowledgments

We thank the members of flow cytometry core facility of the Robert H. Lurie Comprehensive Cancer Center of Northwestern University, Chicago, for assistance with the FACS analysis.

References

1. Herman JG, Baylin SB. Gene silencing in cancer in association with promoter hypermethylation. N Engl J Med 2003;349:2042–54.
2. Laird PW. Cancer epigenetics. Hum Mol Genet 2005;14 Spec No 1:R65–76.
3. Egger G, Liang G, Aparicio A, Jones PA. Epigenetics in human disease and prospects for epigenetic therapy. Nature 2004;429:457–63.
4. Rosato RR, Grant S. Histone deacetylase inhibitors: insights into mechanisms of lethality. Expert Opin Ther Targets 2005;9:809–24.
5. Ungerstedt JS, Sowa Y, Xu WS, et al. Role of thioredoxin in the response of normal and transformed cells to histone deacetylase inhibitors. Proc Natl Acad Sci U S A 2005;102:673–8.
6. Xu WS, Parmigiani RB, Marks PA. Histone deacetylase inhibitors: molecular mechanisms of action. Oncogene 2007;26:5541–52.
7. Ruefli AA, Ausserlechner MJ, Bernhard D, et al. The histone deacetylase inhibitor and chemotherapeutic agent suberoylanilide hydroxamic acid (SAHA) induces a cell-death pathway characterized by cleavage of Bid and production of reactive oxygen species. Proc Natl Acad Sci U S A 2001;98:10833–8.
8. Xu W, Ngo L, Perez G, Dokmanovic M, Marks PA. Intrinsic apoptotic and thioredoxin pathways in human prostate cancer cell response to histone deacetylase inhibitor. Proc Natl Acad Sci U S A 2006;103:15540–5.
9. Rosato RR, Almenara JA, Grant S. The histone deacetylase inhibitor MS-275 promotes differentiation or apoptosis in human leukemia cells through a process regulated by generation of reactive oxygen species and induction of p21CIP1/WAF1 1. Cancer Res 2003;63:3637–45.
10. Adimoolam S, Sirisawad M, Chen J, Thiemann P, Ford JM, Buggy JJ. HDAC inhibitor PCI-24781 decreases RAD51 expression and inhibits homologous recombination. Proc Natl Acad Sci U S A 2007;104:19482–7.
11. Buggy JJ, Cao ZA, Bass KE, et al. CRA-024781: a novel synthetic inhibitor of histone deacetylase enzymes with antitumor activity *in vitro* and *in vivo*. Mol Cancer Ther 2006;5:1309–17.
12. S. D. Undevia LJ, RL, Schilsky D, Loury S, Balasubramanian C, Mani M, Sirisawad JJ, Buggy RA, Miller MJ, Ratain. Phase I study of the safety, pharmacokinetics (PK) and pharmacodynamics (PD) of the histone deacetylase inhibitor (HDACi) PCI-24781. In: J Clin Oncol; 2008; 2008. p. (May 20 suppl; abstr 14514).
13. Perez-Galan P, Roue G, Villamor N, Montserrat E, Campo E, Colomer D. The proteasome inhibitor bortezomib induces apoptosis in mantle-cell lymphoma through generation of ROS and Noxa activation independent of p53 status. Blood 2006;107:257–64.
14. Yu C, Rahmani M, Dent P, Grant S. The hierarchical relationship between MAPK signaling and ROS generation in human leukemia cells undergoing apoptosis in response to the proteasome inhibitor Bortezomib. Exp Cell Res 2004;295:555–66.
15. Ling YH, Liebes L, Zou Y, Perez-Soler R. Reactive oxygen species generation and mitochondrial dysfunction in the apoptotic response to Bortezomib, a novel proteasome inhibitor, in human H460 non-small cell lung cancer cells. J Biol Chem 2003;278:33714–23.
16. Adachi M, Zhang Y, Zhao X, et al. Synergistic effect of histone deacetylase inhibitors FK228 and m-carboxycinnamic acid bis-hydroxamide with proteasome inhibitors PSI and PS-341 against gastrointestinal adenocarcinoma cells. Clin Cancer Res 2004;10:3853–62.
17. Feng R, Oton A, Mapara MY, Anderson G, Belani C, Lentzsch S. The histone deacetylase inhibitor, PXD101, potentiates bortezomib-induced anti-multiple myeloma effect by induction of oxidative stress and DNA damage. Br J Haematol 2007;139:385–97.
18. Heider U, von Metzler I, Kaiser M, et al. Synergistic interaction of the histone deacetylase inhibitor SAHA with the proteasome inhibitor bortezomib in mantle cell lymphoma. Eur J Haematol 2008;80:133–42.
19. Miller CP, Ban K, Dujka ME, et al. NPI-0052, a novel proteasome inhibitor, induces caspase-8 and ROS-dependent apoptosis alone and in combination with HDAC inhibitors in leukemia cells. Blood 2007;110:267–77.
20. Dai Y, Chen S, Kramer LB, Funk VL, Dent P, Grant S. Interactions between bortezomib and romidepsin and belinostat in chronic lymphocytic leukemia cells. Clin Cancer Res 2008;14:549–58.
21. Evens AM, Lecane P, Magda D, et al. Motexafin gadolinium generates reactive oxygen species and induces apoptosis in sensitive and highly resistant multiple myeloma cells. Blood 2005;105:1265–73.
22. Chandra J, Tracy J, Loegering D, et al. Adaphostin-induced oxidative stress overcomes BCR/ABL mutation-dependent and -independent imatinib resistance. Blood 2006;107:2501–6.
23. Cao ZA, Bass KE, Balasubramanian S, et al. CRA-026440: a potent, broad-spectrum, hydroxamic histone deacetylase inhibitor with antiproliferative and antiangiogenic activity *in vitro* and *in vivo*. Mol Cancer Ther 2006;5:1693–701.
24. Chou TC, Talalay P. Quantitative analysis of dose-effect relationships: the combined effects of multiple drugs or enzyme inhibitors. Adv Enzyme Regul 1984;22:27–55.
25. Zamzami N, Marchetti P, Castedo M, et al. Inhibitors of permeability transition interfere with the disruption of the mitochondrial transmembrane potential during apoptosis. FEBS Lett 1996;384:53–7.
26. Henry-Mowatt J, Dive C, Martinou JC, James D. Role of mitochondrial membrane permeabilization in apoptosis and cancer. Oncogene 2004;23:2850–60.
27. Richon VM, Sandhoff TW, Rifkind RA, Marks PA. Histone deacetylase inhibitor selectively induces p21WAF1 expression and gene-associated histone acetylation. Proc Natl Acad Sci U S A 2000;97:10014–9.
28. Blagosklonny MV, Robey R, Sackett DL, et al. Histone deacetylase inhibitors all induce p21 but differentially cause tubulin acetylation, mitotic arrest, and cytotoxicity. Mol Cancer Ther 2002;1:937–41.
29. Chai F, Evdokiou A, Young GP, Zalewski PD. Involvement of p21(Waf1/Cip1) and its cleavage by DEVD-caspase during apoptosis of colorectal cancer cells induced by butyrate. Carcinogenesis 2000;21:7–14.
30. Goy A, Younes A, McLaughlin P, et al. Phase II study of proteasome inhibitor bortezomib in relapsed or refractory B-cell non-Hodgkin's lymphoma. J Clin Oncol 2005;23:667–75.
31. Blum KA, Johnson JL, Niedzwiecki D, Canellos GP, Cheson BD, Bartlett NL. Single agent bortezomib in the treatment of relapsed and refractory Hodgkin lymphoma: cancer and leukemia Group B protocol 50206. Leuk Lymphoma 2007;48:1313–9.
32. Karin M, Cao Y, Greten FR, Li ZW. NF-κB in cancer: from innocent bystander to major culprit. Nature reviews 2002;2:301–10.
33. Rao PH, Houldsworth J, Dyomina K, et al. Chromosomal and gene amplification in diffuse large B-cell lymphoma. Blood 1998;92:234–40.
34. Dai Y, Rahmani M, Grant S. An intact NF-kappaB pathway is required for histone deacetylase inhibitor-induced G1 arrest and maturation in U937 human myeloid leukemia cells. Cell Cycle 2003;2:467–72.
35. Oh GS, Pae HO, Lee BS, et al. Hydrogen sulfide inhibits nitric oxide production and nuclear factor-kappaB via heme oxygenase-1 expression in RAW264.7 macrophages stimulated with lipopolysaccharide. Free Radic Biol Med 2006;41:106–19.
36. Chaea HJ, Kim HR, Kang YJ, et al. Heme oxygenase-1 induction by (S)-enantiomer of YS-51 (YS-51S), a synthetic isoquinoline alkaloid, inhibits nitric oxide production and nuclear factor-êB translocation in ROS 17/2.8 cells activated with inflammatory stimulants. Int Immunopharmacol 2007;7:1559–68.
37. Hamamura RS, Ohyashiki JH, Kurashina R, et al. Induction of heme oxygenase-1 by cobalt protoporphyrin enhances the antitumour effect of bortezomib in adult T-cell leukaemia cells. Br J Cancer 2007;97:1099–105.
38. Bubici C, Papa S, Dean K, Franzoso G. Mutual cross-talk between reactive oxygen species and nuclear factor-kappa B: molecular basis and biological significance. Oncogene 2006;25:6731–48.
39. Taylor WR, Stark GR. Regulation of the G2/M transition by p53. Oncogene 2001;20:1803–15.
40. Dejligbjerg M, Grauslund M, Christensen IJ, Tjornelund J, Buhl Jensen P, Sehested M. Identification of predictive biomarkers for the histone deacetylase inhibitor belinostat in a panel of human cancer cell lines. Cancer Biomark 2008;4:101–9.